International Journal of Heat and Mass Transfer 79 (2014) 796–806

Contents lists available at ScienceDirect

International Journal of Heat and Mass Transfer

journal homepage: www.elsevier.com/locate/ijhmt

Application of the weighted-sum-of-gray-gases model for media composed of arbitrary concentrations of H_2O, CO_2 and soot

Fabiano Cassol [a], Rogério Brittes [a], Francis H.R. França [a,*], Ofodike A. Ezekoye [b]

[a] Department of Mechanical Engineering, Federal University of Rio Grande do Sul, Rua Sarmento Leite, 425, 90050-170 Porto Alegre, RS, Brazil
[b] Department of Mechanical Engineering, University of Texas at Austin, 204 East Dean Keeton Street, 78712 Austin, TX, USA

ARTICLE INFO

Article history:
Received 24 April 2014
Received in revised form 15 July 2014
Accepted 12 August 2014
Available online 17 September 2014

Keywords:
Radiative heat transfer
Participating gases
Soot
Weighted-sum-of-gray-gases

ABSTRACT

The weighted-sum-of-gray-gases (WSGG) model is widely used in engineering computations of radiative heat transfer in participating media due to its relatively simple implementation and reasonable accuracy. However, a major difficulty arises with its application to general gas mixtures where the mole ratios of the participating components are not constant. The present study presents a WSGG methodology to allow efficient, accurate computation of radiative heat transfer in mixtures of H_2O, CO_2, and soot with arbitrary concentrations. The method is based on first establishing independent correlations for each species, which are then combined to form the WSGG correlations for the mixture. A few test cases are presented to assess the accuracy of the two methods by comparisons with benchmark solutions obtained with the line-by-line integration (LBL) of the spectrum.

1. Introduction

Predictions of heat transfer in combustion processes require a detailed analysis of thermal radiation in participating gases at high temperatures. In combustion systems, radiation strongly affects the temperature field, and consequently the reaction kinetics. On the other hand, solving radiation in combustion gases requires accounting for the highly complex dependence of the absorption coefficient with the wavenumber, especially under the conditions of steep variations in the temperature and concentrations of the participating species. The absorption coefficient of participating gases, such as H_2O and CO_2, can involve hundreds of thousands or millions of transition lines with steep variations across the spectrum. Although line-by-line (LBL) integration of the spectral lines can provide solutions with high level of accuracy, its application to global combustion codes, which involve coupled solutions of chemical kinetics, turbulent flow field and energy conservation, is prohibitively demanding for most practical applications. Moreover, since the solution of the other phenomena also introduces errors and uncertainties, it seems more reasonable to make use of gas models that can efficiently integrate the radiative transfer equation over the spectrum with an acceptable level of uncertainty.

Gas models have been an ever present research field in radiation in participating media. The gray gas model, which assumes that the absorption coefficient is independent of the wavenumber, cannot provide reliable results when radiation in gases such as H_2O and CO_2 is important. Probably the most widely employed method, the weighted-sum-of-gray-gases (WSGG) [1] replaces the spectrum with a few gray gases and transparent windows. Typically, the absorption coefficient and the weighting factor of each gray gas are obtained from fitting data of total emittance for different temperatures and pressure path-lengths. The conceptual simplicity of the WSGG model allows its application together with any method of spatial integration of the RTE [2]. Most of the modern gas models, which make direct use of the spectral lines generated from detailed spectral database, have proposed improvements and generalizations to the WSGG model, such as the spectral-line-based WSGG (SLW) [3–9], the absorption distribution function (ADF) [10–12], the cumulative wavenumber (CW) [13,14], the full spectrum correlated-k (FSCK) [15,16], and the multi-scale FSCK (MSFSCK) [17].

For all gas models, the major challenge is to make accurate predictions of the radiative transfer under conditions of steep variations in the temperature and molar concentrations of the participating species. In flames, for example, not only the molar concentrations of the participating species vary from point to point in the domain, but also the mole ratio between the species. Evaluation of the gas models against LBL benchmark solutions for a set of non-isothermal, non-homogeneous problems have been presented for the FSCK [15], the MSFSCK [17], the SLW [9], and WSGG [18]. Interestingly, the errors of the WSGG model reported

* Corresponding author. Fax: +55 51 3308 3222.
E-mail address: frfranca@mecanica.ufrgs.br (F.H.R. França).

http://dx.doi.org/10.1016/j.ijheatmasstransfer.2014.08.032
0017-9310/

in [18] were of comparable magnitude to those obtained with more sophisticated methods. However, in typical implementations of the WSGG model, the correlations were developed for constant mole fraction ratios of H_2O and CO_2 (2/1 and 1/1) [19–21]. In recent times, a few WSGG correlations have been proposed to allow for the variation in the mole ratio of H_2O and CO_2 [22,23]. However, such an approach adds another dimension to the WSGG correlations, which in turn introduces one more source of error to the model. Also, other participating species (soot, for instance) could be present in the mixture, so generating correlations to cover all possible combinations of mole ratios does not seem a viable task.

This paper presents a WSGG approach to consider arbitrary concentrations of the participating species, allowing for local variations in their mole ratios, and the inclusion of any number of participating species. The method is based on the generation of WSGG correlations for individual species, which are then superposed to form the correlations of the mixture. In particular, it considers mixtures of H_2O, CO_2 and soot, but the methodology can be extended to any set of participating species. The WSGG correlations for H_2O and CO_2 were obtained from spectral lines generated from HITEMP2010, the latest source of data for H_2O and CO_2 at high temperatures, while for soot a well-known linear dependence with wavenumber was utilized. The methodology is tested against LBL benchmark solutions considering a set of test cases, which includes non-isothermal, non-homogeneous media with varying mole ratio between the species. The results show that the superposition WSGG model can provide accurate results, while still keeping the efficiency and simplicity of the traditional WSGG model.

2. Physical and mathematical modeling

Radiation heat transfer in participating media is governed by the radiative transfer equation (RTE), which establishes a relation for the variation of the spectral radiation intensity I_η along a certain path in the medium. Considering absorption and emission, but neglecting scattering, the variation in the spectral intensity can be determined by:

$$\frac{dI_\eta}{dx} = -\kappa_{\eta,m}(x)I_\eta(x) + \kappa_{\eta,m}(x)I_{\eta b}(x) \tag{1}$$

where η is the wavenumber, x is the distance from the wall, $\kappa_{\eta,m}$ is the mixture spectral absorption coefficient, and $I_{\eta b}$ is the blackbody spectral intensity at the temperature in position x, given by Planck's distribution law. In Eq. (1), the index m was used for $\kappa_{\eta,m}$ to consider that the medium is formed with a mixture of H_2O, CO_2 and soot. In this case, it can be obtained by:

$$\kappa_{\eta,m}(x) = \kappa_{\eta,w}(x) + \kappa_{\eta,c}(x) + \kappa_{\eta,s}(x) \tag{2}$$

where the subscripts w, c and s stand for H_2O, CO_2 and soot, respectively. The explicit spatial dependence is retained to more clearly present the formulation for problems in which the spectral absorption coefficient varies along the position x due to variations in the local temperature and/or concentrations of the participating species. In spite of the presence of soot, radiation scattering is not considered in Eq. (1) since scattering effects in soot are of minor significance in comparison to absorption and emission under the conditions of the present study [24].

The global solution of the radiative transfer requires the spatial and the spectral integrations of Eq. (1). In this study, the spatial integration is carried out with the discrete ordinates method, although any other method could be applied. The discrete ordinates solve the RTE for a set of discrete directions that span a total solid angle of 4π. The continuous integral over the solid angle is approximated by a numerical quadrature scheme, in which the equations are solved for a series of L directions. Eq. (1), in the framework of the discrete ordinates method, can be written for positive and negative directions according to:

$$\mu_l \frac{dI^+_{\eta,l}}{dx} = -\kappa_{\eta,m}(x)I^+_{\eta,l}(x) + \kappa_{\eta,m}(x)I_{\eta b}(x) \tag{3a}$$

$$-\mu_l \frac{dI^-_{\eta,l}}{dx} = -\kappa_{\eta,m}(x)I^-_{\eta,l}(x) + \kappa_{\eta,m}(x)I_{\eta b}(x) \tag{3b}$$

where μ_l is the directional cosine towards l direction ($1 \leqslant l \leqslant L$). Fig. 1 depicts the positive and negative intensities in direction l and position x for the one-dimensional medium slab that will be considered in the present study. Considering that the medium is bounded by black walls, the boundary conditions for Eqs. (3a) and (3b) are $I^+_{\eta,l}(x=0) = I_{\eta b}(x=0)$ and $I^-_{\eta,l}(x=X) = I_{\eta b}(x=X)$.

Once the intensities are solved for each discrete position x and direction l, the volumetric radiative heat source (W/m^3) and the radiative heat flux (W/m^2) can be determined respectively by:

$$\dot{q}_R(x) = \sum_{l=1}^{L} \int_\eta \left\{ 2\pi\kappa_{\eta,m}(x)w_l \left[I^+_{\eta,l}(x) + I^-_{\eta,l}(x) \right] - 4\pi\kappa_{\eta,m}(x)I_{\eta b}(x) \right\} d\eta \tag{4a}$$

$$q''_R(x) = \sum_{l=1}^{L} \int_\eta 2\pi w_l \mu_l \left[I^+_{\eta,l}(x) - I^-_{\eta,l}(x) \right] d\eta \tag{4b}$$

It follows directly from the set of Eqs. (3)-(4) that the volumetric radiative heat source corresponds to the divergence of the radiative heat flux but with the opposite sign, that is, $\dot{q}_R(x) = -dq''_R(x)/dx$.

The solution of the volumetric radiative heat source and the radiative heat flux in Eqs. (4a) and (4b) still requires the integration over the wavenumber η, which is carried out in this study by means of the weighted-sum-of-gray-gases (WSGG) model. In the next section, a methodology is proposed for the application of the WSGG model for non-isothermal, non-homogeneous media composed of arbitrary concentrations H_2O, CO_2 and soot. Prior to this discussion, the line-by-line (LBL) integration of the RTE for the evaluation of the WSGG approach is reviewed.

2.1. Line-by-line (LBL) integration

The LBL integration can be taken as the benchmark solution to evaluate spectral models, except for some minor errors that may arise in the numerical integration of the RTE in space and in the generation of the spectral absorption coefficient. In the LBL integration, the RTE is solved for each spectral absorption coefficient according to Eqs. (3a) and (3b). This requires the knowledge of the local spectral absorption coefficients of the species that form the mixture, H_2O, CO_2 and soot.

In this study, the HITEMP2010 database [25] was used for the generation of the spectral absorption coefficients for H_2O and CO_2, $\kappa_{\eta,w}$ and $\kappa_{\eta,c}$, setting a spectral resolution of 0.067 cm^{-1} for the wavenumber range between 0 and 10,000 cm^{-1}. This corresponds to 150,000 wavenumber values around which the spectral lines were computed from Lorentz profile [26]. Complementary tests showed that reducing the spectral resolution to 0.025 cm^{-1} did not lead to significant changes in the results. The spectral database was generated for the partial pressures of 0.01, 0.1, 0.2 and 0.4 atm for H_2O, using linear interpolation for partial pressures

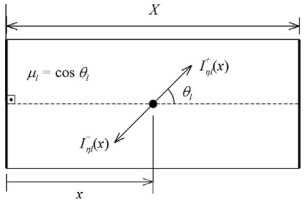

Fig. 1. Schematic of the one-dimensional medium slab bounded by black walls.

between these values. For CO_2, the spectral lines were generated for a partial pressure of 1.0 atm, and a simple linear relation was applied for other partial pressures, since CO_2 does not present a self-broadening effect. In the same way, to avoid generating the spectral lines for every temperature in the nodal points of numerical integration, which would be excessively time consuming, the spectra were generated with interval of 100 K between the ranges of temperatures considered in this study (i.e., from 400 K to 1800 K). For other temperatures, the spectrum was obtained by linear interpolation of the spectra generated between 400 K and 1800 K. This procedure greatly reduced the computational time without introducing significant errors in the LBL solutions. More details on the approach to generate the spectral absorption coefficients for H_2O and CO_2 are discussed in [18].

As for soot particulate, empirical observations indicate that its spectral absorption coefficient has a simple linear variation with the wavenumber [26–29], according to:

$$\kappa_{\eta,s}(x) = f_v(x)\alpha\eta \tag{5}$$

where $f_v(x)$ is the local volumetric fraction of soot, and α is a dimensionless constant that depends of the fuel: $\alpha = 6.3$ for combustion oil, 4.9 for propane, 4.0 for acetylene, 3.7–7.5 for coal combustion, and 4.1 for methane flames [30].

2.2. The WSGG model

The WSGG model represents the entire spectrum with a few gray gases with uniform absorption coefficient, $\kappa_{\chi,j}$, and transparent windows, as seen in Fig. 2. For any given condition, the medium is represented by a total of J_χ gray gases. Index χ represents the medium component: H_2O ($\chi = w$), CO_2 ($\chi = c$), soot ($\chi = s$), or the mixture itself ($\chi = m$). Each gray gas can also be characterized by its pressure absorption coefficient $\kappa_{p\chi,j}$, defined as $\kappa_{p\chi,j} = \kappa_{\chi,j}/p_\chi$, where p_χ is the partial pressure of the participating species χ. Very important to the WSGG model is the assumption that the spectral location (characterized by $\eta_{\chi,j}$ and $\Delta\eta_{\chi,j}$ in the figure) as well as the pressure absorption coefficient $\kappa_{p\chi,j}$ of each gray gas does not depend on the medium temperature and on the partial pressure of the participating species. These simplifications play a key role in the treatment of non-isothermal, non-homogeneous media.

Considering that the spectrum of the mixture ($\chi = m$) can be represented by the sketch in Fig. 2, the integration of Eqs. (3a) and (3b) in the spectral interval $\Delta\eta_{m,j}$ leads to:

$$\mu_l \frac{dI^+_{m,j,l}}{dx} = -\kappa_{m,j}(x)I^+_{m,j,l}(x) + \kappa_{m,j}(x)a_{m,j}(x)I_b(x) \tag{6a}$$

$$-\mu_l \frac{dI^-_{m,j,l}}{dx} = -\kappa_{m,j}(x)I^-_{m,j,l}(x) + \kappa_{m,j}(x)a_{m,j}(x)I_b(x) \tag{6b}$$

where $I^+_{m,j,l}$ and $I^-_{m,j,l}$ are the integrated intensities over $\Delta\eta_{m,j}$, and $a_{m,j}(x)$ is the fraction of the blackbody energy, at the temperature

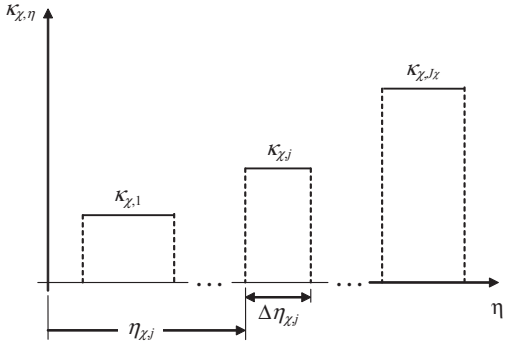

Fig. 2. Schematic of the gray gas model for a given species.

of the medium in position x, that is emitted in interval $\Delta\eta_{m,j}$. The boundary conditions for Eqs. (6a) and (6b) are $I^+_{m,j,l}(x=0) = a_{m,j}(T_{x=0})I_b(x=0)$ and $I^-_{m,j,l}(x=X) = a_{m,j}(T_{x=X})I_b(x=X)$.

The integration of the volumetric radiative heat source and the radiative heat flux in Eqs. (4a) and (4b) with the WSGG model leads to:

$$\dot{q}_R(x) = \sum_{l=1}^{L}\sum_{j=1}^{J_m} 2\pi\kappa_{m,j}(x)w_l\left\{\left[I^+_{m,j,l}(x) + I^-_{m,j,l}(x)\right] - 2a_{m,j}(x)I_b(x)\right\} \tag{7a}$$

$$q''_R(x) = \sum_{l=1}^{L}\sum_{j=0}^{J_m} 2\pi w_l\mu_l\left[I^+_{m,j,l}(x) - I^-_{m,j,l}(x)\right] \tag{7b}$$

The transparent windows ($j = 0$) need to be considered in the computation of the radiative heat flux in Eq. (7b), but they play no role in the solution of the radiative heat source with Eq. (7a). The WSGG model is intrinsically conservative, so computing the radiative heat source and heat flux as above will necessarily lead to $\dot{q}_R(x) = -dq''_R(x)/dx$.

Eqs. (7a) and (7b) are closed form solutions of the radiation heat transfer in a medium composed of a mixture of participating species. The apparent simplicity of the formulation belies the fact that it still requires the knowledge of the WSGG parameters for the mixture, that is, the absorption coefficient $\kappa_{m,j}$ and the weighting factor (temperature coefficient) $a_{m,j}$ of each gray gas, as well as the number of gray gases J_m. The next sections present one approach that allows the determination of these parameters from the knowledge of the WSGG coefficients of the individual components.

2.2.1. The standard WSGG method

The WSGG model, depicted in Fig. 2, makes a quite simple representation of the spectral absorption coefficient of participating gases such as H_2O and CO_2, which can be represented by hundreds of thousands or millions of spectral lines. In practice, the gray gas parameters, that is the pressure absorption coefficient, $\kappa_{p\chi,i}$, and the temperature coefficient, $a_{\chi,i}$, are obtained from fitting global radiation data. For instance, the total emittance of a given component χ along a certain path of length X is defined as:

$$\varepsilon_\chi = \frac{\int_\eta I_{\eta b}\left[1 - \exp\left(-\kappa_{p\chi,\eta}p_\chi X\right)\right]d\eta}{\sigma T^4/\pi} \tag{8}$$

where $\kappa_{p\chi,\eta}$ is the spectral pressure absorption coefficient, $\kappa_{p\chi,\eta} = \kappa_{\chi,\eta}/p_\chi$. Appling the WSGG model in the integration of Eq. (8) leads to the following relation for the total emittance:

$$\varepsilon_\chi = \sum_{j=1}^{J_\chi} a_{\chi,j}(T)\left[1 - \exp\left(-\kappa_{p\chi,j}p_\chi X\right)\right] \tag{9}$$

Next, the total emittance in Eq. (8) can be computed with the LBL integration of the spectrum for a set of temperatures, T, and pressure path lengths, $p_\chi X$. Then, Eq. (9) can be used to fit values for the pressure absorption coefficients, $\kappa_{p\chi,j}$, and for the polynomial coefficients of the temperature dependent coefficients $a_{\chi,j}$, according to:

$$a_{\chi,j}(T) = \sum_{k=1}^{K_\chi} b_{\chi,j,k}T^{k-1} \tag{10}$$

In addition to the gray gases, the WSGG postulates the existence of transparent windows for which the absorption coefficient is null, that is, $\kappa_{\chi,0} = 0$. For the energy to be conserved, the temperature coefficients need to satisfy the following relation:

$$\sum_{j=0}^{J_\chi} a_{\chi,j}(T) = 1 \tag{11}$$

The above relation provides a method to find the temperature coefficient for the transparent windows, $a_{\chi,0}(T)$, from the knowledge of the temperature coefficients of the gray gases ($1 \leqslant j \leqslant J_\chi$):

$$a_{\chi,0}(T) = 1 - \sum_{j=1}^{J_\chi} a_{\chi,j}(T) \tag{12}$$

One limitation of the typical WSGG correlations available in the literature is that the fitting coefficients are generated for specific mole ratios (or partial pressure ratios) of the participant components. For instance, in [18,19] the coefficients were obtained for partial pressures ratios of $p_w/p_c = 1$ and 2. Table 1 reproduces the WSGG coefficients presented in [18] for $p_w/p_c = 2$, obtained from data generated from HITEMP2010. The coefficients in Table 1 will be used in the present study together with the proposed methodologies in a few comparative test problems. In this case, the participating species is represented with the index $\chi = wc$. The drawback of generating the coefficients for a specific partial pressures ratio is that it can vary both locally and on average. Moreover, the presence of soot with different relative concentrations with respect to H_2O and CO_2 makes it infeasible to generate the WSGG correlations to cover all possible mixtures. The next section presents a WSGG methodology to model mixtures with arbitrary relative concentrations of the participating gases, based on individual species correlations, which are combined to generate a mixture correlation.

2.2.2. WSGG correlations for individual species

H_2O and CO_2 Tables 2 and 3 present the WSGG coefficients for H_2O ($\chi = w$) and CO_2 ($\chi = c$), respectively, which were obtained from fitting total emittance data computed from LBL integration of spectral absorption lines generated from HITEMP2010. The adopted procedure to generate the coefficients was the same as applied in [18]. Figs. 3 and 4 compare the total emittance computed from the LBL integration and from the use of the correlations. In general, the correlations provide a good fit of the total emittance data, except for H_2O at the lowest value of the pressure path length, $p_wX = 0.01$ atm m. However, in such conditions, the radiative heat transfer is of minor importance, so the error should not cause a major impact in global calculations. In Tables 2 and 3, four gray gases were used. It was verified in a complementary study, not shown here, that increasing the number of gray gases did not cause a significant modification in the results. In the same way, for both gases, a fourth order polynomial relation ($K_w = K_c = 5$) in Eq. (10) proved to be sufficient for an accurate fitting of the temperature coefficients.

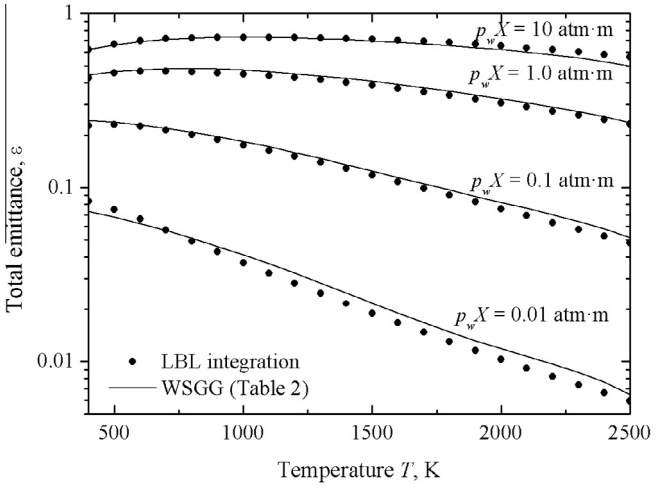

Fig. 3. Comparison of the total emittance of H_2O computed by LBL integration and by the WSGG model with the coefficients of Table 2.

Soot In general, soot is generated in fuel rich regions of flames with concentrations and emission characteristics that depend on the fuel. For methane flames, for instance, the soot volumetric fraction typically varies between 10^{-7} and 10^{-5} (0.1–10 ppm). Soot

Table 1
WSGG coefficients for H_2O/CO_2 mixtures with $p_w/p_c = 2$ [18].

j	$\kappa_{p,wc,j}$ (atm m)$^{-1}$	$b_{wc,j,1}$	$b_{wc,j,2}$ (K^{-1})	$b_{wc,j,3}$ (K^{-2})	$b_{wc,j,4}$ (K^{-3})	$b_{wc,j,5}$ (K^{-4})
1	0.192	0.05617	78.44×10^{-5}	-85.63×10^{-8}	42.46×10^{-11}	-74.4×10^{-15}
2	1.719	0.14260	17.95×10^{-5}	-1.077×10^{-8}	-6.971×10^{-11}	17.74×10^{-15}
3	11.370	0.13620	25.74×10^{-5}	-37.11×10^{-8}	15.70×10^{-11}	-22.67×10^{-15}
4	111.016	0.12220	-2.327×10^{-5}	-7.492×10^{-8}	4.275×10^{-11}	-6.608×10^{-15}

Valid for temperatures between 400 and 2500 K and 0.001 atm m $\leqslant (p_w + p_c)X \leqslant$ 10 atm m.

Table 2
WSGG coefficients for H_2O with four gray gases.

j	$\kappa_{p,w,j}$ (atm m)$^{-1}$	$b_{w,j,1}$	$b_{w,j,2}$ (K^{-1})	$b_{w,j,3}$ (K^{-2})	$b_{w,j,4}$ (K^{-3})	$b_{w,j,5}$ (K^{-4})
1	0.171	0.06617	55.48×10^{-5}	-48.41×10^{-8}	22.27×10^{-11}	-40.17×10^{-15}
2	1.551	0.11045	0.576×10^{-5}	24.00×10^{-8}	-17.01×10^{-11}	30.96×10^{-15}
3	5.562	−0.04915	70.63×10^{-5}	-70.12×10^{-8}	26.07×10^{-11}	-34.94×10^{-15}
4	49.159	0.23675	-18.91×10^{-5}	-0.907×10^{-8}	4.082×10^{-11}	-8.778×10^{-15}

Valid for temperatures between 400 and 2500 K and 0.001 atm m $\leqslant p_wX \leqslant$ 10 atm m.

Table 3
WSGG coefficients for CO_2 with four gray gases.

j	$\kappa_{p,c,j}$ (atm m)$^{-1}$	$b_{c,j,1}$	$b_{c,j,2}$ (K^{-1})	$b_{c,j,3}$ (K^{-2})	$b_{c,j,4}$ (K^{-3})	$b_{c,j,5}$ (K^{-4})
1	0.138	0.09990	64.41×10^{-5}	-86.94×10^{-8}	41.27×10^{-11}	-67.74×10^{-15}
2	1.895	0.00942	10.36×10^{-5}	-2.277×10^{-8}	-2.134×10^{-11}	6.497×10^{-15}
3	13.301	0.14511	-30.73×10^{-5}	37.65×10^{-8}	-18.41×10^{-11}	30.16×10^{-15}
4	340.811	−0.02915	25.23×10^{-5}	-26.10×10^{-8}	9.965×10^{-11}	-13.26×10^{-15}

Valid for temperatures between 400 and 2500 K and 0.001 atm m $\leqslant p_cX \leqslant$ 10 atm m.

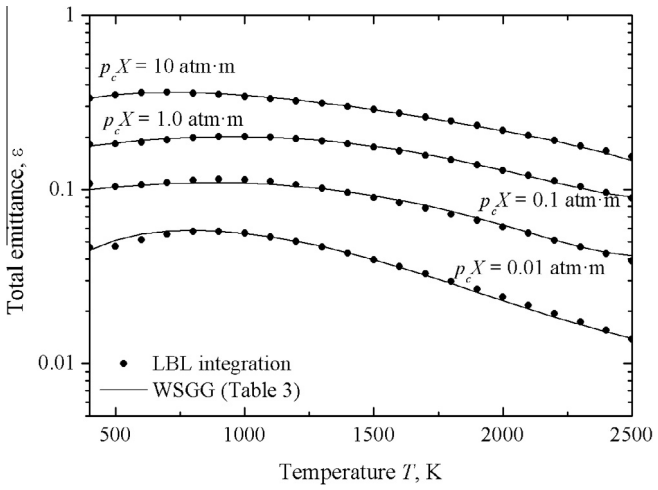

Fig. 4. Comparison of the total emittance of CO_2 computed by LBL integration and by the WSGG model with the coefficients of Table 3.

particles can be quite small, with characteristic dimensions of 100–1 μm, so soot can be considered to be at the local gas temperature, with a continuous emission in the infrared region of the spectrum. Experiments show that soot has a much higher radiative emission than gases, which makes it important to solve soot radiation in combustion modeling even when its concentration is relatively small.

Tables 4–6 present the WSGG absorption coefficients and the temperature dependent coefficients for soot ($\chi = s$) considering 2, 3 and 4 gray gases, respectively. Since it is more common to present the concentration of soot by its volumetric fraction f_v rather than its partial pressure. Tables 4–6 provide values for the volumetric fraction absorption coefficient $\kappa_{f_v,s,j}$, so that the absorption coefficient of soot can be computed by $\kappa_{s,j}(x) = f_v(x)\alpha\kappa_{f_v,s,j}$. Fig. 5 compares the emittance data obtained with WSGG model with 2, 3 and 4 gray gases. As seen, while 2 and 3 gray gases can lead to poor accuracy, 4 gray gases proved to make satisfactory fitting of the total emittance data with the exception of very high temperatures, above 2000 K. As with H_2O and CO_2, a fourth order polynomial relation, $K_s = 5$, led to a good fit of the temperature dependent coefficients. There is no transparent window for soot, therefore $a_{s,0} = 0$.

3. Applying the WSGG model to H_2O, CO_2 and soot mixtures

The major difficulty in combining WSGG correlations of different species is that there is no clear relation between the gray gases coefficients and their position in the spectrum. Although Fig. 2 represents gray gases covering specific regions of the spectrum, this is only a physical argument to simplify the spectral integration of the RTE, and to establish a fitting equation for total emittance, as given by Eq. (9). Once the coefficients are fitted from data of total emittance, it is simply not meaningful trying to establish the regions of the spectrum that are associated with each gray gas, defined by $\eta_{\chi,j}$ and $\Delta\eta_{\chi,j}$ in Fig. 2.

However, another physical argument can be used to combine the WSGG coefficients of different species. In fact, the temperature coefficient $a_{\chi,j}$ can be alternatively interpreted as the probability that the energy of the blackbody is emitted in the region of the spectrum where the absorption coefficient is $\kappa_{p,\chi,j}$. Therefore, the probability that the gray gas absorption coefficient of the mixture is the sum of a given combination of the gray gas absorption coefficients of the components will be equal to the product of their respective probabilities. In other words, for a mixture of H_2O, CO_2 and soot:

$$\kappa_{m,j_m}(x) = \kappa_{w,j_w}(x) + \kappa_{c,j_c}(x) + \kappa_{s,j_s}(x) \quad (13a)$$

$$a_{m,j_m}(x) = a_{w,j_w}(x) \times a_{c,j_c}(x) \times a_{s,j_s}(x) \quad (13b)$$

The above relation is similar to an early implementation of the WSGG model combining H_2O and CO_2 (with fixed mole ratio) with soot [31] and is similar to the SLW treatment of mixtures of H_2O and CO_2 that was proposed in [8].

Table 4
WSGG coefficients for soot with two gray gases.

j	$\kappa_{fv,s,j}$ $(m)^{-1}$	$b_{s,j,1}$	$b_{s,j,2}$ (K^{-1})	$b_{s,j,3}$ (K^{-2})	$b_{s,j,4}$ (K^{-3})	$b_{s,j,5}$ (K^{-4})
1	22313.49	0.95552	-1.431×10^{-3}	9.871×10^{-7}	-3.390×10^{-10}	4.555×10^{-14}
2	466624.8	0.08010	1.290×10^{-3}	-7.874×10^{-7}	2.322×10^{-10}	-3.084×10^{-14}

Valid for temperatures between 400 and 2500 K.

Table 5
WSGG coefficients for soot with three gray gases.

j	$\kappa_{fv,s,j}$ $(m)^{-1}$	$b_{s,j,1}$	$b_{s,j,2}$ (K^{-1})	$b_{s,j,3}$ (K^{-2})	$b_{s,j,4}$ (K^{-3})	$b_{s,j,5}$ (K^{-4})
1	1251.56	0.02812	-1.271×10^{-4}	1.395×10^{-7}	-5.672×10^{-11}	8.068×10^{-15}
2	50470.6	1.25626	-18.74×10^{-4}	12.09×10^{-7}	-39.89×10^{-11}	52.85×10^{-15}
3	460361.0	−0.25179	18.55×10^{-4}	-11.39×10^{-7}	34.46×10^{-11}	-45.58×10^{-15}

Valid for temperatures between 400 and 2500 K.

Table 6
WSGG coefficients for soot with four gray gases.

j	$\kappa_{fv,s,j}$ $(m)^{-1}$	$b_{s,j,1}$	$b_{s,j,2}$ (K^{-1})	$b_{s,j,3}$ (K^{-2})	$b_{s,j,4}$ (K^{-3})	$b_{s,j,5}$ (K^{-4})
1	2875.86	0.00129	-0.545×10^{-5}	0.123×10^{-7}	-0.847×10^{-11}	1.6807×10^{-15}
2	39234.9	1.26110	-319.2×10^{-5}	27.72×10^{-7}	-100.5×10^{-11}	132.8×10^{-15}
3	160748.0	−0.25757	362.1×10^{-5}	-40.12×10^{-7}	154.9×10^{-11}	-207.8×10^{-15}
4	495898.0	0.07980	-72.08×10^{-5}	15.87×10^{-7}	-70.89×10^{-11}	97.69×10^{-15}

Valid for temperatures between 400 and 2500 K.

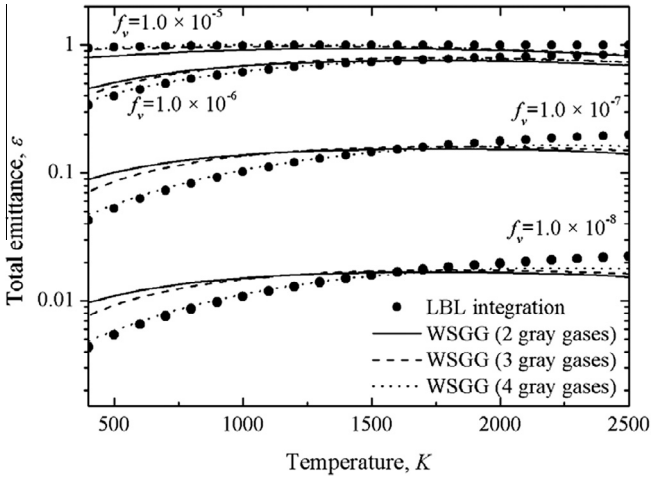

Fig. 5. Comparison of the total emittance of soot computed by LBL integration and by the WSGG model with the coefficients of Table 4-6.

In Eqs. (13a) and (13b), the transparent windows of H_2O and CO_2 ($\kappa_{w,0} = 0$ and $\kappa_{c,0} = 0$) have to be considered, so $0 \leqslant j_w \leqslant J_w$, $0 \leqslant j_c \leqslant J_c$. On the other hand, there are no transparent windows for soot, that is $a_{s,0} = 0$, so $1 \leqslant j_s \leqslant J_s$. For the mixture, the number of gray gases will be therefore $J_m = (J_w + 1) \times (J_c + 1) \times J_s$. In the correlations provided in this study for H_2O and CO_2, $J_w = J_c = 4$. If correlations with 4 gray gases are used for soot ($J_s = 4$), then $J_m = 100$, but J_m can be reduced to 75 and 50 if 3 or 2 gray gases are used for soot, respectively. It follows from Eqs. (11) and (13b) that:

$$\sum_{j=0}^{J_m} a_j(T) = 1 \tag{14}$$

The above relations can be readily extended to more components with the same probabilistic argument. Moreover, if one of the above components is not present one needs to simply suppress the respective coefficients of Eqs. (13a) and (13b). For instance, for mixtures of H_2O and CO_2 without soot:

$$\kappa_{m,j_m}(x) = \kappa_{w,j_w}(x) + \kappa_{c,j_c}(x) \tag{15a}$$
$$a_{m,j_m}(x) = a_{w,j_w}(x) \times a_{c,j_c}(x) \tag{15b}$$

In this case, $J_m = (J_w + 1) \times (J_c + 1) - 1 = 24$, discounting the transparent windows ($m = 0$).

3.1. Solution methodology

This study will present a set of radiative heat transfer problems in one-dimensional medium slabs formed with mixtures of H_2O, CO_2 and soot, bounded by black walls. The problems will be solved with the LBL integration as well as with the superposition WSGG model. The temperature distribution, $T(x)$, the molar concentrations of H_2O and CO_2, $Y_w(x)$ and $Y_c(x)$, and the soot volumetric fraction, $f_v(x)$, are specified. The partial pressures of H_2O and CO_2 are, therefore, computed as $p_w(x) = pY_w(x)$ and $p_c(x) = pY_c(x)$, in which p is the total pressure of the medium, and Y_i is the mole fraction of species i.

In the superposition WSGG model, the steps below are followed:

(i) The local gray gas absorption coefficients of each species are computed by:

$$\kappa_{w,j}(x) = p_w(x)\kappa_{p,w,j} \tag{16a}$$
$$\kappa_{c,j}(x) = p_c(x)\kappa_{p,c,j} \tag{16b}$$
$$\kappa_{s,j}(x) = f_v(x)\alpha\kappa_{f_v,s,j} \tag{16c}$$

where the pressure absorption coefficients of H_2O and CO_2, $\kappa_{p,w,j}$ and $\kappa_{p,c,j}$, are taken from Tables 2 and 3 respectively, while the volumetric fraction absorption coefficient of soot, $\kappa_{f_v,s,j}$, is taken from Table 4–6 depending on the number of gray gases that are considered for soot.

(ii) Next, the gray gas temperature coefficients of each species, $a_{w,j_w}(x)$, $a_{c,j_c}(x)$ and $a_{s,j_s}(x)$, are computed according to Eqs. (10) using the local temperature $T(x)$ and the polynomial coefficients of Table 2–6.

(iii) The local gray gas absorption coefficient, $\kappa_{m,j}(x)$, and the temperature coefficient, $a_{m,j}(x)$, of the mixture are computed by Eqs. (13a) and (13b), or by Eqs. (15a) and (15b) if no soot is present.

(iv) The RTE for the positive and negative directions are computed from Eqs. (6a) and (6b) for each gray gas, and finally the radiative heat source and heat flux are computed from Eqs. (7a) and (7b).

Finally, to further evaluate the superposition WSGG model, the test problems will also be solved with the use of the coefficients obtained in [18] for a fixed pressure ratio of $p_w/p_c = 2$, shown in Table 1. In this case, the gray gas absorption coefficient, $\kappa_{m,j}(x)$, and the temperature coefficient, $a_{m,j}(x)$, of the mixture will be computed with the following relations:

$$\kappa_{m,j_m}(x) = \kappa_{wc,j_{wc}}(x) + \kappa_{s,j_s}(x) \tag{17a}$$
$$a_{m,j_m}(x) = a_{wc,j_{wc}}(x) \times a_{s,j_s}(x) \tag{17b}$$

in which $\kappa_{wc,j} = (p_w + p_c)\kappa_{p,wc,j}$, with $\kappa_{p,wc,j}$ and $a_{wc,j}$ being taken from Table 1.

4. Results

The proposed solution methodology is presented for the one-dimensional geometry shown in Fig. 1, consisting of two flat plates having emissivity equal to 1 (black walls). The plates are separated by the distance $X = 1$ m, a representative length scale for some combustion systems. When soot is present, the constant α in equation (5) will be set equal to 4.1, a typical value for soot generated in methane flames. The physical domain between the two black surfaces was divided into 200 equal-sized elements. The discrete ordinates method (DOM) was applied to $L = 30$ directions, using a Gauss–Legendre quadrature. These numerical settings led to grid-independent solutions. The total pressure of the system is $p = 1$ atm.

Six test cases will be solved to evaluate the accuracy of the superposition WSGG approach described in this paper. The accuracy of the solutions will be assessed by means of the relative deviation between the radiative heat sources and the heat fluxes obtained with the LBL integration and with the WSGG methods, according to:

$$\delta = \left| \frac{\dot{q}_{R,\mathrm{WSGG}} - \dot{q}_{R,\mathrm{LBL}}}{\max\left(\dot{q}_{R,\mathrm{LBL}}\right)} \right| \times 100\% \tag{18a}$$

$$\gamma = \left| \frac{q''_{R,\mathrm{WSGG}} - q''_{R,\mathrm{LBL}}}{\max\left(q''_{R,\mathrm{LBL}}\right)} \right| \times 100\% \tag{18b}$$

where δ and γ are the relative errors for the radiative heat source and for the radiative heat flux, while $\max(\dot{q}_{R,\mathrm{LBL}})$ and $\max(q''_{R,\mathrm{LBL}})$ are the maximum absolute values of the radiative heat source and of the radiative heat flux, as computed by the LBL integration.

4.1. Test case 1

The medium is considered to be isothermal and homogeneous, being composed of 20% H_2O ($Y_w = 0.2$), 10% CO_2 ($Y_c = 0.1$), but no

soot ($f_v = 0$). The remaining species in the medium corresponds to inert gas. The medium temperature is 1100 K, and the walls are kept at 400 K.

Fig. 6(a) and (b) show, respectively, the radiative heat source and heat flux computed with the LBL integration and with the two WSGG approaches: using the coefficients obtained in [18] for a fixed mole ratio of H_2O and CO_2, labeled as WSGG ($p_w/p_c = 2$), and applying the superposition of the individual WSGG coefficients for H_2O and CO_2. As seen, the radiative heat source is negative in the entire domain, since every point in the medium, at 1100 K, loses energy in balance to the cold walls, at 400 K. In its absolute value, the radiative heat source increases with the proximity of the walls, as it happens with the radiative heat flux, which falls to zero at the mid distance between the plates due to symmetry. Comparing the results, one observes that the standard and the superposition WSGG methods provided a satisfactory agreement with the LBL benchmark solution. Table 7 presents the average and maximum relative deviations for the radiative heat source and heat flux, grouped as Case 1. Thus, the superposition method competes well with the standard WSGG model, which was specifically developed for the mole ratio considered in this problem, $Y_w/Y_c = 2$. Since soot was not present, the number of gray gases for the superposition method was 24 against the 4 gray gases of the standard method, which corresponds to six times more computational effort. However, the clear advantage of the full superposition WSGG method is that it is not limited to a specific mole ratio, as is the case of the standard method.

Table 7
Maximum and average errors of the different WSGG models.

	δ_{max} (%)	$\delta_{average}$ (%)	γ_{max} (%)	$\gamma_{average}$ (%)
Case 1				
Standard ($p_w/p_c = 2$)	7.5	0.3	2.3	0.2
Superposition	2.8	1.0	7.6	3.1
Case 2				
Standard ($p_w/p_c = 2$)	9.3	3.9	6.0	2.0
Superposition	10.5	3.9	9.8	5.3
Case 3				
Standard ($p_w/p_c = 2$)	21.0	9.7	8.7	3.6
Superposition	11.2	6.4	7.2	2.9
Case 4				
Superposition $J_s = 2$	7.6	2.5	4.3	1.6
Superposition $J_s = 3$	4.3	2.0	1.8	1.1
Superposition $J_s = 4$	4.3	1.3	2.3	1.0
Case 5				
Superposition $J_s = 2$	7.9	2.1	3.2	1.2
Superposition $J_s = 3$	4.6	1.5	2.6	1.2
Superposition $J_s = 4$	4.6	1.3	2.2	1.0
Case 6				
Superposition $J_s = 2$	11.7	3.8	6.3	5.2
Superposition $J_s = 3$	12.6	4.0	6.6	5.4
Superposition $J_s = 4$	2.9	1.5	2.3	1.6

4.2. Test case 2

The medium has the same uniform composition as in Case 1 ($Y_w = 0.2$, $Y_c = 0.1$, and $f_v = 0$), but the temperature is non-uniform, varying according to the following relation:

$$T(x) = 400\ \mathrm{K} + (1400\ \mathrm{K}) \sin^2\left(\frac{2\pi x}{X}\right) \tag{19}$$

With the above equation, the temperature rises from 400 K on the walls to 1800 K for $x/X = 0.25$ and 0.75, and then falls to 400 K at the mid distance between the plates, $x/X = 0.5$.

The radiative heat source and heat flux obtained with the LBL integration and the two WSGG approaches are shown in Fig. 7(a) and (b). The absolute value of the radiative heat source presents two peaks in the same positions where the medium temperature reaches the highest value, at $x/X = 0.25$ and 0.75. In the cold regions of the medium, the radiative heat source is positive, indicating net gain of radiation from the hot regions. The radiative heat flux exhibits a symmetric profile, reaching the highest absolute values at $x/X = 0.125$ and 0.825, where the temperature gradient is maximum. Overall, the two WSGG approaches led to the correct trends for both the radiative heat source and heat flux. The maximum and relative errors are presented in Table 7, grouped as Case 2. The moderate increase in the error, when compared to the isothermal problem in the previous case, can be attributed to the high temperature gradient, which reaches a value as high as 8800 K/m.

4.3. Test case 3

In Cases 1 and 2, the standard WSGG with $p_w/p_c = 2$ led to satisfactory comparisons with the LBL solution, since the pressure ratio was maintained at this value for all points of the domain. However, in computation of flames, the mole ratio can vary considerably when more realistic chemistry and transport are modeled. It is expected that in such cases the correlations obtained for constant pressure ratios are no longer accurate. To illustrate this

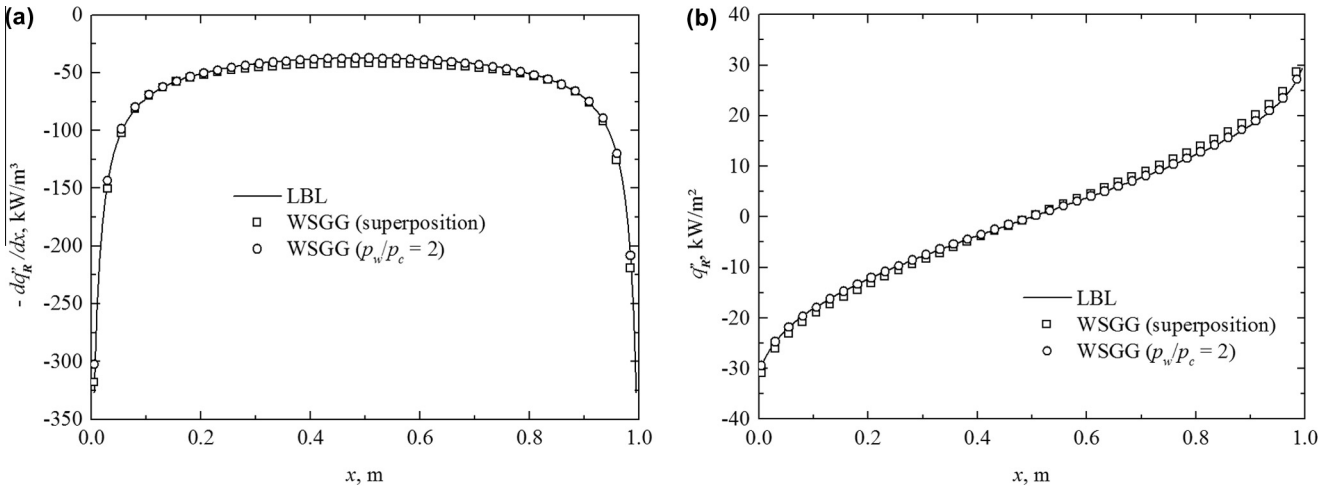

Fig. 6. Comparison of the solutions obtained by the LBL integration and the different WSGG models for Case 1: (a) radiative heat source. (b) Radiation heat flux.

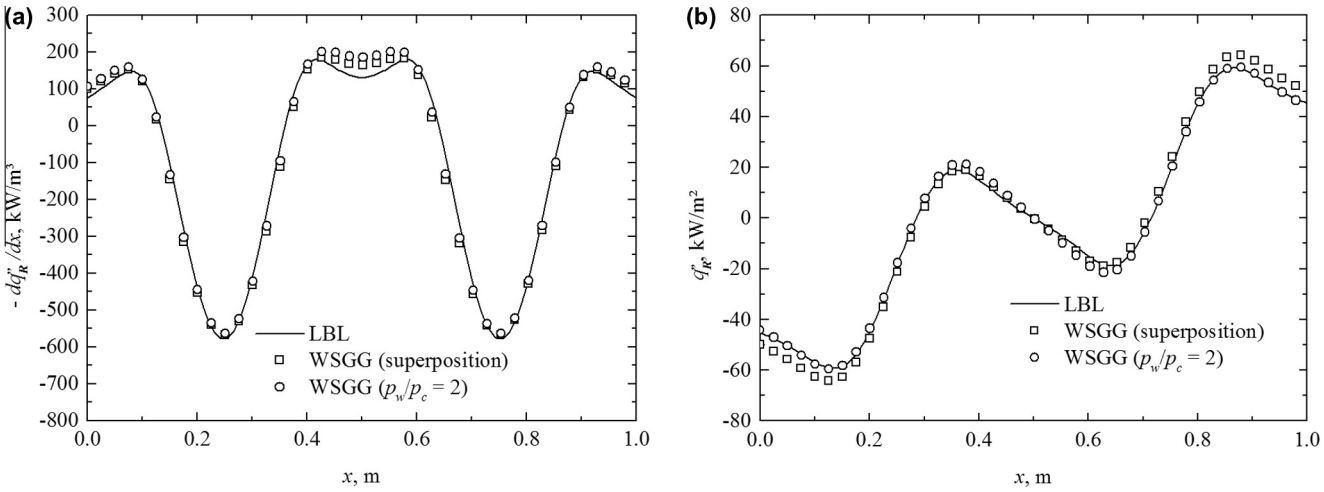

Fig. 7. Comparison of the solutions obtained by the LBL integration and the different WSGG models for Case 2: (a) radiative heat source. (b) Radiation heat flux.

condition, Case 3 assumes variable molar ratios. The medium temperature and the molar concentrations of H_2O and CO_2 vary according to the following relations:

$$T(x) = 400 + 1400\sin^2\left(\frac{\pi x}{X}\right) \tag{20a}$$

$$Y_w(x) = 0.2\sin^2\left(\frac{2\pi x}{X}\right) \tag{20b}$$

$$Y_c(x) = 0.1\cos^2\left(\frac{2\pi x}{X}\right) \tag{20c}$$

With the above relations, the molar ratio between H_2O and CO_2 is not constant, although on average the ratio p_w/p_c remains equal to 2 in the domain. The temperature in this case rises from 400 K on the walls to 1800 K in the mid distance between the walls, $x/X = 0.5$. Therefore, contrary to the previous case, there is only one peak in the medium temperature.

The radiative heat source and the heat flux are presented in Fig. 8(a) and (b). In this case, the maximum absolute value of the radiative heat source is not coincident with the position where the medium temperature is the highest, since the variation in the molar concentrations of the participating species does not follow the temperature. One observes that the standard WSGG with $p_w/p_c = 2$ overpredicted the absolute value of the radiative heat source in the mid distance between the plates ($x/X = 0.5$). In fact, when using this correlation, it is assumed that the mole ratio between H_2O and CO_2 is 2/1 in all positions in the medium, while in fact the concentration of H_2O is much smaller than that of CO_2 in the mid of the slab. According to Eqs. (20b) and (20c), $Y_w/Y_c \to 0$ for $x/X \to 0.5$. Since H_2O is a more effective absorber-emitter than CO_2, the use of the standard WSGG correlation with $p_w/p_c = 2$ inevitably overpredicts the radiation exchanges in this region. The opposite effect takes place in the vicinity of $x/X = 0.2$ and 0.8, where the use of the standard WSGG model with $p_w/p_c = 2$ underpredicted the actual amount of H_2O, leading to an underestimation of the absorption of radiation from the higher temperature regions in the medium. As seen in Table 7, Case 3, the maximum error when using the standard WSGG model was 21% for the computation of the radiative heat source. With the superposition method, the errors remained at about 10% or less, and captured well the behaviors of the radiative heat source and heat flux even for this difficult test case, as can be seen in Fig. 8(a) and (b).

4.4. Test case 4

For Case 4, the medium is assumed to contain soot with a constant volumetric fraction $f_v = 1.0 \times 10^{-6}$, a typical concentration in the combustion of methane, and uniform concentrations of H_2O ($Y_w = 0.2$) and CO_2 ($Y_c = 0.1$). The temperature distribution is non-uniform, as given by Eq. (19), with peaks at $x/X = 0.25$ and 0.75.

Fig. 9(a) and (b) compare the radiative heat source and heat flux as obtained by the LBL integration and the superposition method, in the latter considering 2, 3 and 4 gray gases for soot according to the coefficients in Tables 4–6. As seen, the results are similar to those in Fig. 7(a) and (b), with the difference that the presence of soot increased the magnitudes of radiative heat source and heat flux. All superposition solutions led to accurate predictions of the radiation heat transfer in media containing H_2O, CO_2 and soot, which is corroborated by the average and maximum errors in Table 7 (Case 4). The improvement was expected: since radiation is dominated by soot, which presents a much simpler spectral behavior than H_2O and CO_2, the problem can be more easily solved with the WSGG model. It is interesting that using 2 and 3 gray gases for soot could lead to satisfactory comparisons to the LBL solution, in spite of not providing an overall good accuracy in the computation of the total emittance, as seen in Fig. 5. The reason for the good performance is the fact that the soot volumetric fraction of $f_v = 1.0 \times 10^{-6}$ can be well solved with 2 and 3 gray gases for soot, especially for temperatures around the maximum temperature reached in the medium, 1800 K (Fig. 5). Clearly, using less gray gases for soot is advantageous, in the sense that the mixture is modeled with a smaller number of gray gases. As discussed in Section 3, when using 2, 3 and 4 gray gases for soot, the number of gray gases for the mixture are $J_m = 50$, 75 and 100, respectively.

4.5. Test case 5

This case is similar to Case 4, with the exception that the concentrations of H_2O and CO_2, and soot are non-uniform, and equal to:

$$Y_w(x) = 0.2\sin^2\left(\frac{2\pi x}{X}\right) \tag{21a}$$

$$Y_c(x) = 0.1\sin^2\left(\frac{2\pi x}{X}\right) \tag{21b}$$

$$f_v(x) = 1.0 \times 10^{-6}\sin^2\left(\frac{2\pi x}{X}\right) \tag{21c}$$

With the above relations, the concentrations of H_2O, CO_2 and soot rise from 0 at the walls to the maximum values of $Y_{w,\max} = 0.2$, $Y_{c,\max} = 0.1$, and $f_{v,\max} = 1.0 \times 10^{-6}$ for $x/X = 0.25$ and 0.75, and then fall to zero at the mid distance between the plates, $x/X = 0.5$.

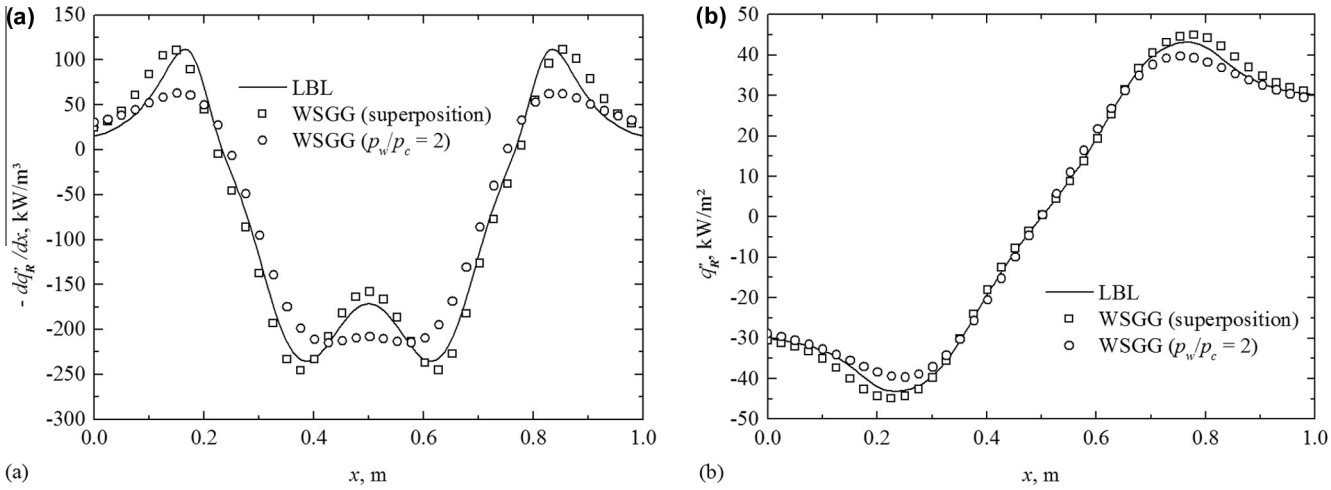

Fig. 8. Comparison of the solutions obtained by the LBL integration and the different WSGG models for Case 3: (a) radiative heat source. (b) Radiation heat flux.

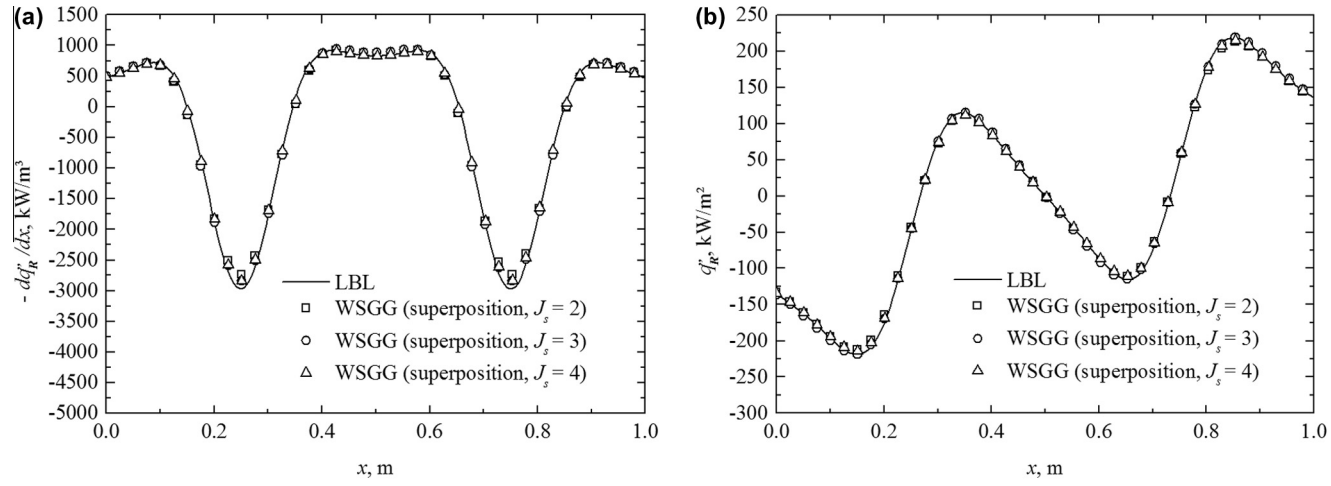

Fig. 9. Comparison of the solutions obtained by the LBL integration and the different WSGG models for Case 4: (a) radiative heat source. (b) Radiation heat flux.

The results for this case are shown in Fig. 10(a) and (b). In most of the domain, the radiative heat source resembles the one in Case 4, with exception of the regions close to the walls and in the mid distance between the plates, where the radiative to zero falls to zero. In fact, since the medium is nearly transparent in these regions ($\kappa_m \to 0$ for $x/X \to 0$, 0.5 and 1), the radiative heat source should necessarily fall to zero. On the other hand, although the average concentrations of the participating species are half of those in Case 4, the heat flux on the wall increases, because the low temperature regions of the medium are less absorbing, so more heat can be transferred from the high temperature regions to the walls. Fig. 10(a) and (b) indicate that the use of 2, 3 and 4 gray gases for soot again provided good results, which is corroborated by the values of the errors in Table 7 (Case 5).

4.6. Test case 6

In the previous two cases, radiation was dominated by soot in all points of the domain. In computation of flames, however, it is common that soot is concentrated in a limited part of the domain, so that in some regions radiation may be dominated by soot, while in others by gases such as H_2O and CO_2. To exemplify such a situation, it is considered that the concentrations of H_2O, CO_2 and soot are described for the following relations:

$$Y_w(x) = 0.2\sin^2\left(\frac{2\pi x}{X}\right) \tag{22a}$$

$$Y_c(x) = 0.1\sin^2\left(\frac{2\pi x}{X}\right) \tag{22b}$$

$$f_v(x) = 0, \text{ for } 0 \leqslant x/X < 0.25 \text{ and } 0.75 < x/X \leqslant 1 \tag{22c}$$

$$f_v(x) = 1.0\times 10^{-6}\sin^2\left[\frac{2\pi(x-0.25)}{X}\right], \quad \text{for } 0.25 < x/X < 0.75 \text{ peak at } x/X = 0.5 \tag{22d}$$

The medium temperature is uniform and equal 1100 K, while the walls are kept at 400 K. In this case, the radiation should be dominated by H_2O and CO_2 in the positions between $0 \leqslant x/X < 0.25$ and $0.75 < x/X \leqslant 1$, and by soot in the positions between $0.25 < x/X < 0.75$. Fig. 11(a) and (b) show that the solution with 4 gray gases for soot can provide accurate solutions for the radiative heat source and heat flux, as also indicated by the maximum and average error in Table 7. On the other hand, the use of the correlations with 2 and 3 gray gases for soot led to a poor estimation of the radiative heat source in the mid distance between the plates. This can be explained by inspecting Fig. 5. For medium temperatures in the order of 1100 K, the use of soot correlations with 2 and 3 gray gases overestimated soot emission, which is what happens in the mid region of the slab. This result warns that the use of soot correlation with 2 and 3 gray gases can lead to poor accuracy in some cases, and

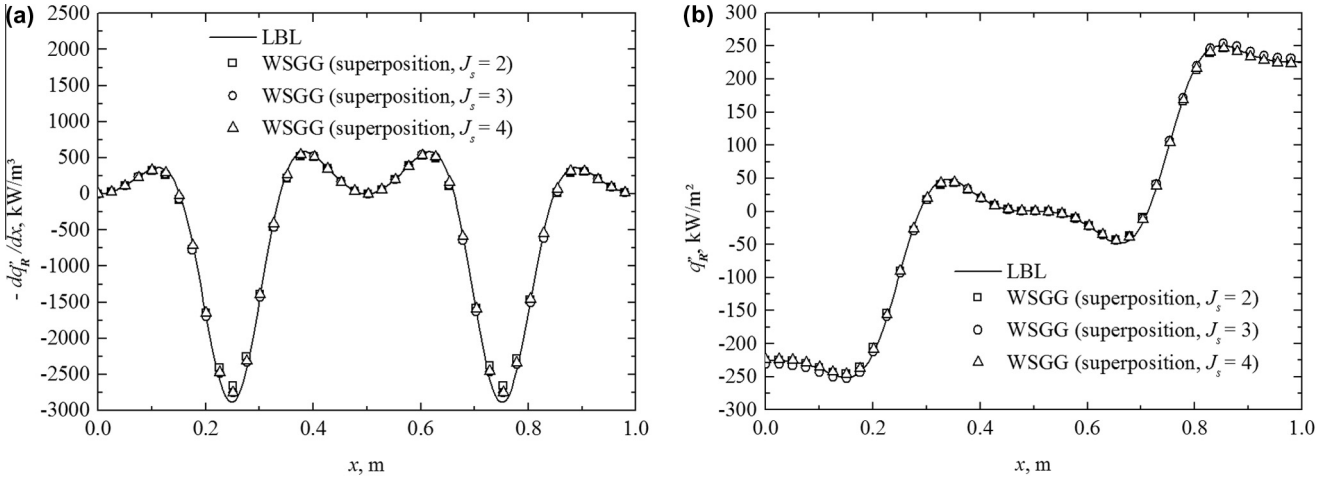

Fig. 10. Comparison of the solutions obtained by the LBL integration and the different WSGG models for Case 5: (a) radiative heat source. (b) Radiation heat flux.

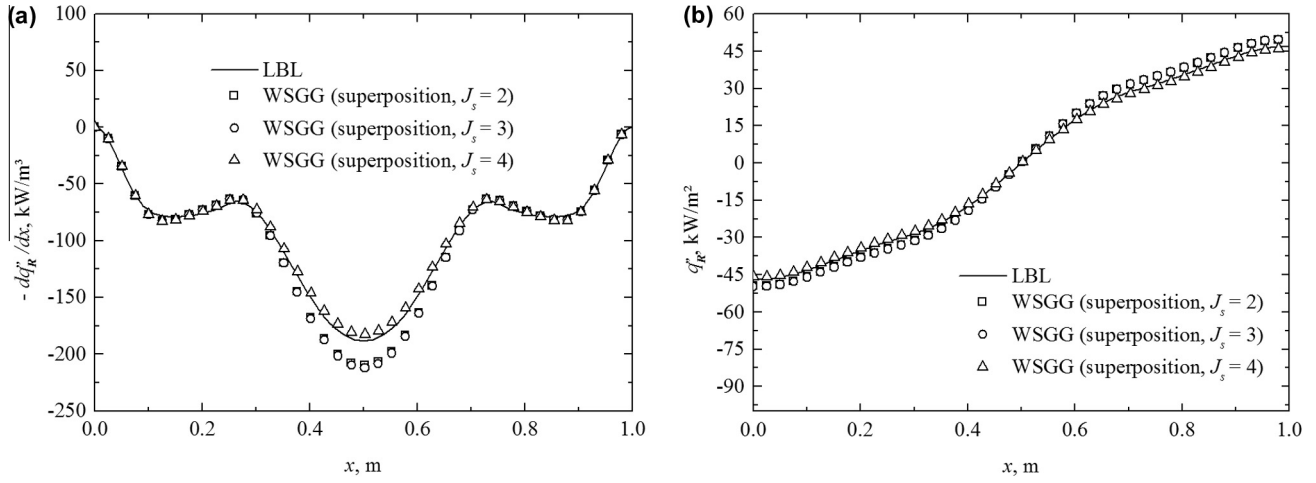

Fig. 11. Comparison of the solutions obtained by the LBL integration and the different WSGG models for Case 6: (a) radiative heat source. (b) Radiation heat flux.

their use should be limited to the physical conditions where the emittance is well evaluated by those correlations. The use of 4 gray gases for soot led to accurate results for all cases, and is recommended when a wide range of temperatures and volumetric fractions of soot is involved.

5. Conclusions

This study presented the application of the weighted-sum-of-gray-gases (WSGG) model to solve radiative heat transfer in mixtures with arbitrary concentrations of the participating species. In particular, it was considered that the medium was composed of H_2O, CO_2 and soot, but the method can be readily extended to more species. The methodology is based on the use of independent WSGG correlations, which are then superposed to solve general problems in which the mole ratio between the species is not constant, a known limitation of the standard WSGG model. The superposition method proved reliable in all test cases, which included non-isothermal, non-homogeneous with non-constant mole ratios between the species. The superposition WSGG model is robust, intrinsically conservative and of relatively simple implementation. Although the number of gray gases of the mixture can substantially increase with the superposition, the method is still computationally efficient. For instance, in the case with 100 gray gases to solve mixtures of H_2O, CO_2 and soot, the computational time was only 0.1% of the time required by the LBL solution.

Conflict of interest

None declared.

Acknowledgments

FC and RB thank the financial support from CAPES and CNPq through a doctorate scholarship grant. FHRF thanks CNPq (Brazil) for research Grants 309961/2013-0 and 476490/2013-8.

References

[1] H.C. Hottel, A.F. Sarofim, Radiative Transfer, McGraw-Hill, New York, 1967.
[2] M.F. Modest, The weighted-sum-of-gray-gases model for arbitrary solution methods in radiative transfer, J. Heat Transfer 113 (3) (1991) 650–656.
[3] M.K. Denison, B.W. Webb, A spectral line based weighted-sum-of-gray-gases model for arbitrary RTE solvers, J. Heat Transfer 115 (4) (1993) 1004–1012.
[4] M.K. Denison, B.W. Webb, The spectral line-based weighted-sum-of-gray-gases model in non-isothermal nonhomogeneous media, J. Heat Transfer 117 (2) (1995) 359–365.
[5] V.P. Solovjov, B.W. Webb, Global spectral methods in gas radiation: the exact limit of the SLW model and its relationship to the ADF and FSK methods, J. Heat Transfer 133 (4) (2011). 042701(1–9).

[6] M.K. Denison, B.W. Webb, An absorption-line blackbody distribution function for efficient calculation of total gas radiative transfer, J. Quant. Spectrosc. Radiat. Transfer 50 (5) (1993) 499–510.
[7] M.K. Denison, B.W. Webb, Development and application of an absorption line blackbody distribution function for CO_2, Int. J. Heat Mass Transfer 38 (10) (1995) 1813–1821.
[8] M.K. Denison, B.W. Webb, The spectral-line weighted-sum-of-gray-gases model for H_2O/CO_2 mixtures, J. Heat Transfer 117 (3) (1995) 788–792.
[9] V.P. Solovjov, D. Lemonnie, B.W. Webb, SLW-1 modeling of radiative heat transfer in nonisothermal nonhomogeneous gas mixtures with soot, J. Heat Transfer 133 (10) (2011). 102701(1–9).
[10] P. Rivière, A. Soufiani, M.Y. Perrin, H. Riad, A. Gleizes, Air mixture radiative property modelling in the temperature range 10,000–40,000 K, J. Quant. Spectrosc. Radiat. Transfer 56 (1) (1996) 29–46.
[11] L. Pierrot, P. Rivière, A. Soufiani, J. Taine, A fictitious-gas-based absorption distribution function global model for radiative transfer in hot gases, J. Quant. Spectrosc. Radiat. Transfer 62 (5) (1999) 609–624.
[12] L. Pierrot, A. Soufiani, J. Taine, Accuracy of narrow-band and global models for radiative transfer in H_2O, CO_2, and H_2O–CO_2 mixtures at high temperature, J. Quant. Spectrosc. Radiat. Transfer 62 (5) (1999) 523–548.
[13] V.P. Solovjov, B.W. Webb, A local-spectrum correlated model for radiative transfer in non-uniform gas media, J. Quant. Spectrosc. Radiat. Transfer 73 (2–5) (2002) 361–373.
[14] M.M. Galarça, A. Mossi, F.H.R. França, A modification of the cumulative wavenumber method to compute the radiative heat flux in non-uniform media, J. Quant. Spectrosc. Radiat. Transfer 112 (3) (2011) 384–393.
[15] M.F. Modest, H. Zhang, The full-spectrum correlated-*k* distribution for thermal radiation from molecular gas–particulates mixtures, J. Heat Transfer 124 (1) (2002) 30–38.
[16] M.F. Modest, V. Singh, Engineering correlations for full spectrum *k*-distribution of H_2O from HITEMP spectroscopic databank, J. Quant. Spectrosc. Radiat. Transfer 93 (1–3) (2005) 263–271.
[17] H. Zhang, M.F. Modest, A multi-scale full-spectrum correlated-*k* distribution for radiative heat transfer in inhomogeneous gas mixtures, J. Quant. Spectrosc. Radiat. Transfer 73 (2–5) (2002) 349–360.
[18] L.J. Dorigon, G. Duciak, R. Brittes, F. Cassol, M. Galarça, F.H.R. França, WSGG correlations based on HITEMP2010 for computation of thermal radiation in non-isothermal, non-homogeneous H_2O/CO_2 mixtures, Int. J. Heat Mass Transfer 64 (2013) 863–873.
[19] T.F. Smith, Z.F. Shen, J.N. Friedman, Evaluation of coefficients for the weighted sum of gray gases model, J. Heat Transfer 104 (4) (1982) 602–608.
[20] C. Yin, L.C.R. Johansen, L. Rosendahl, S.K. Kaer, New weighted sum of gray gases model applicable to computational fluid dynamics (CFD) modeling of oxy-fuel combustion: derivation, validation, and implementation, Energy Fuels 24 (12) (2010) 6275–6282.
[21] R. Johansson, K. Andersson, B. Leckner, H. Thunman, Models for gaseous radiative heat transfer applied to oxy-fuel conditions in boilers, Int. J. Heat Mass Transfer 53 (1–3) (2010) 220–230.
[22] R. Johansson, B. Leckner, K. Andersson, F. Johnsson, Account for variations in the H_2O to CO_2 molar ratio when modelling gaseous radiative heat transfer with the weighted-sum-of-grey-gases model, Combust. Flame 158 (5) (2011) 893–901.
[23] T. Kangwanpongpan, F.H.R. França, R.C. da Silva, P.S. Schneider, H.J. Krautz, New correlations for the weighted-sum-of-gray-gases in oxy-fuel conditions based on HITEMP 2012 database, Int. J. Heat Mass Transfer 55 (2012) 7419–7433.
[24] M.F. Modest, Radiative Heat Transfer, second ed., Academic Press, New York, 2003.
[25] L.S. Rothman, I.E. Gordon, R.J. Barber, H. Dothe, R.R. Gamache, A. Goldman, V.I. Perevalov, S.A. Tashkun, J. Tennyson, HITEMP, the high-temperature molecular spectroscopic database, J. Quant. Spectrosc. Radiat. Transfer 111 (15) (2010) 2139–2150.
[26] R. Siegel, J.R. Howell, Thermal Radiation Heat Transfer, fourth ed., Taylor & Francis, New York, 2002.
[27] V.V. Barve, O.A. Ezekoye, N.T. Clemens, Effects of flame lift-off height on soot processes in strongly forced methane-air laminar diffusion flames, in; Proceedings of Thermal Engineering Summer Heat Transfer Conference, Vancouver, British Columbia, 2007, pp. 643–651.
[28] L.H. Dorey, N. Bertier, L. Tessé, F. Dupoirieux, Soot and radiation modeling in laminar ethylene flames with tabulated detailed chemistry, C. R. Méc. 339 (12) (2011) 756–769.
[29] V.P. Solovjov, B.W. Webb, An efficient method for modeling radiative transfer in multicomponent gas mixtures with soot, J. Heat Transfer 123 (3) (2001) 450–457.
[30] S. Yagi, H. Iino, Radiation from soot particles in luminous flames, in: Proceedings of the Eighth Symposium (International) on Combustion, Pasadena, CA, 1961, pp. 288–293.
[31] T.F. Smith, A.M. Al-Turki, K.H. Byun, T.K. Kim, Radiative and conductive transfer for a gas/soot mixture between diffuse parallel plates, J. Thermophys. Heat Transfer 1 (1987) 50–55.